Arabian Journal of Chemistry (2022) **15**, 103593

King Saud University

Arabian Journal of Chemistry

www.ksu.edu.sa
www.sciencedirect.com

ORIGINAL ARTICLE

Facile synthesis of quantum dots metal oxide for photocatalytic degradation of organic hazardous materials and factory effluents

Walied A.A. Mohamed [a,*], Hala H. Abd El-Gawad [b], Saleh D. Mekkey [c], Hoda R. Galal [a], Ammar A. Labib [a]

[a] *Inorganic Chemistry Department, National Research Center, Cairo, Egypt*
[b] *Department of Chemistry, Faculty of Science and Arts, King Khalid University, Mohail, Assir, Saudi Arabia*
[c] *Applied Inorganic Chemistry, Chemistry Department, Faculty of Science Al-Azhar University, Cairo, Egypt*

Received 21 September 2021; accepted 23 November 2021
Available online 30 November 2021

KEYWORDS

Zinc oxide quantum dots;
Precipitation improved process;
Indigo Carmine dye;
Recycle process;
Factory effluents

Abstract Solar photocatalytic behavior of zinc oxide quantum dots (ZQs) was studied and synthesized using a modified precipitation process and characterized using various spectroscopic techniques. HRTEM was used to demonstrate and verify the purity of the prepared quantum dot material and the calculated crystallite size is 4.4 and 5.3 nm for the ZQ1 and ZQ2 samples, respectively. The optical characteristics and the BET analysis of ZQs samples investigated great value for the bandgap energy and the specific surface for ZQS samples. The photodegradation process of Indigo Carmine dye (IC) (one of the commercial organic hazardous materials used in the dying process) by ZQ1 recorded the highest synthetic levels equal to $17.18 \times 10^{-3}S^{-1}$. Also, the ZQ1 sample with the smallest particle size reaches the maximum fluorescence rate by almost 31 % in coumarin photo-oxidation than the ZQ2 sample with the largest particle size. This study included a report of the mineralization of IC dye, 16 investigated factory effluents samples, and their recovery ability for ten replication cycles as a case study in the presence of ZQs by sunlight for two months. These evaluation processes are by TOC analysis and COD measurements.

1. Introduction

For life sustainability, both guiding socioeconomic and manufacturing operations, water is the first essential commodity on Earth. This valuable highly resource is subjected to multiple quality threats every day.

In recent years water contamination has been at the forefront of global issues that need many researchers to find safe and inexpensive ways of eliminating these pollutants and

* Corresponding author at: Photochemistry and Nanomaterials lab - Inorganic Chemistry Department – National Research Centre, Cairo 12622, Egypt.
E-mail addresses: waliedfx@yahoo.com, wa.abdel-ghafar@nrc.sci.org (W.A.A. Mohamed), habduljwaad@kku.edu.sa (H.H. A. El-Gawad).
Peer review under responsibility of King Saud University.

ELSEVIER Production and hosting by Elsevier

https://doi.org/10.1016/j.arabjc.2021.103593

improving water quality for many multiple life usages. A river has different types of microorganisms, ponds, aquifers, streams, or other water sources that have a lot of quantities of poisonous chemical materials run to them. So, water purity decreases and becomes harmful to the environment or humans (Alexandrov et al., 2020; El-Sayed et al., 2019; Kharkwal et al., 2020; Kumar et al., 2021b; Lin et al., 2020; Mohamed et al., 2021; Singh et al., 2019; Vaez and Javanbakht, 2020).

However, organic dyes cause water pollution in several sectors such as cosmetics, fabrics, textiles, or certain medicinal products. These dyes have many environmental and economic threats and can cause many diseases such as skin inflammations, allergic dermatitis, and cancer. Therefore, organic compounds removal safely from multiple water supplies is one of the most important fields for many researchers worldwide. Several water contaminants identification, visualization, and removal/reduction techniques have been certified (Banerjee et al., 2014; Hanna et al., 2014; Liang et al., 2020; Lin et al., 2020; Nandi and Das, 2019).

Recently, the photocatalytic technique is an excellent removal and transform method to a wide variety of toxins from wastewater into zero-risk compounds. As photocatalysts, semiconductor metal oxides are considered fundamental components of photocatalytic technology (Abo Zeid et al., 2020; Kitture et al., 2017; Kumar et al., 2019; Rani and Sahare, 2013; Tanji et al., 2020). Due to its quality, preferably delivering non-toxic end materials and simple operation, this success is related to its outstanding properties such as wide bandgap, environmentally friendly design, low-cost, biocompatibility, and others. Metal oxide quantum dots (MOQDs) with particle sizes less than 10 nm have unique photoluminescent and physicochemical properties. Zinc oxide quantum dots (ZQs) are commonly included in the catalogue of MOQDs as a promising material for different photocatalytic, biological as anticancer, electrical as size-dependence photoluminescence effect (Busseron et al., 2013; Jain et al., 2014; Muşat et al., 2014), nano paint for marine antifouling and wastewater treatment applications (Mohamed et al., 2021; Mohamed et al., 2020).

Both 3D-containing energies and ZQs confinement structure reinforce the physicochemical properties and photoluminescent that primarily depend on the effect of the quantum size. 'particle-in-box' expression describes the relationship between electron structure changes and particle size, especially when the particle size falls on the waviness of electro-short photons. Easy frequency changes depending on decreases in the particles' size are often susceptible to absorption and light emission. (Chen et al., 2019; Khan et al., 2014; Kumar et al., 2021a; Lee et al., 2019; Wang et al., 2017; Zhu et al., 2018). The exciton-radius (electron-hole pair radius) is restricted by reducing its crystal size to the nano-range and known as the quantum size effect. As a consequence of this containment, the excitons gain momentum, which considers the blue-shift observed irradiated from such nanomaterials as a theoretical basis (Ambade et al., 2014; Felbier et al., 2014; Mohammed Ali et al., 2018; Repp and Erdem, 2016; Senger and Bajaj, 2003).

The Indigo Carmine dye is a conventional organic commercial dye for textile manufacturing in the local Egyptian factories because of the low cost and high coloring efficiency. Also, it is tested the photocatalytic behavior of the quantum dots of synthesized zinc oxide (ZQs) prepared under a xenon reactor by the modified precipitation process. Also, this study focuses on the effects of mineralization performance for the Indigo Carmine dye and 16 samples of industrial wastewater and determining the maximum recycling mechanism according to Egyptian environmental law.

The motivation of our work in the near future is to design a prototype for real industrial wastewater treatment by sun light in textile and dyes factories depending on active photocatalysts such ZQs prepared samples which initially succeed with high efficiency during the recycling process for 10 repetition times. Also, prospective future research would provide a local economic strategy for ZQ preparation since there are more exciting application using ZQs as sophisticated advanced optics and QD solar cell applications.

2. Experimental

2.1. Materials

Packages of zinc acetate dihydrate ($Zn(CH_3COO)_2{\cdot}2H_2O$) and sodium hydroxide (NaOH) bought from Merck Company and a commercial pack of nano zinc oxide from Aldrich-Sigma. The chemicals used in this work are also analytical grade and used without further purification, and for all formulated solutions deionized water was used. Indigo Carmine dye (IC) ($C_{16}H_8N_2Na_2O_8S_2$, M. Wt. = 466.36 g/mol) was also obtained from Fluka and picked by one of the largest Spinning & Weaving Egyptian companies as one of the industrial red color dyes used in the dying process.

2.2. Preparation of quantum dots oxides

Using zinc acetate as a starting material and sodium hydroxide solution to add oxygen (O) to the production of quantum dots, ZQs were synthesized via the modified precipitation process. Sodium hydroxide (0·1 M) was applied slowly dropwise (0·5 ml/min) under intense stirring at 9000 rpm to the zinc acetate aqueous solution (0·1 M). The aging reaction has done for 48 h to validate the formation of a dense white precipitate by addition and stability. ZQs isolated by centrifugation and washed until neutral pH (pH = 7) were obtained with deionized water, followed by methanol washing.

For the complete elimination of solvent and any reactive impurities, ZQs samples were dried in an oven at 60 ^{0}C for 24 h. The ZQs (ZQ1 and ZQ2) samples were calcinated after drying in the muffle furnace at 450 and 550 ^{0}C for 20 min, respectively. Eventually, the ZQs samples produced were stored under airtight conditions.

2.3. Characterization

X-ray powder diffraction (XRPD-Philips Holland) was used for phases and crystal structure analysis of the prepared quantum dot catalyst. The Xpert MPD model uses 0.154 nm, 50 kV, and 40 mA copper -K al radiation, and the data recorded is 100 s/step at 0.0170 step size. A high-resolution TEM (A JEOL HRTEM- Philips CM-120) was determined the surface properties of the samples. The bandgap energies for all ZQs prepared samples were determined by UV–vis diffuse reflectance spectra (DRS, Varian Cary 300). Also, Shimadzu 240 spectrometer-

JAPAN was used for determining the absorption spectrum shifts of the chosen dyes.

A spectrophotometer has calculated photoluminescence output (Shimadzu-JAPAN) and from the slope of the relationship between the time curves for fluorescence intensity and irradiation, the apparent rate constant (k_f) was determined. The Brunauer Emmett-Teller (EBT) study measured the surface areas (SA) of the prepared materials. After drying the samples at 150 ^{0}C for 60 min, the SA values (eq. (1)) determined using the Tristar 3000 Micrometrics (Micrometrics apparatus-Norcross-GA) method depended on the adsorption isotherm of N_2 gas as a liquid nitrogen temperature at 77 K.

$$s = \frac{6}{d \times \rho} \quad (1)$$

where s, ρ and d is the specific surface area, density of ZnO (5.63 g/Cm^3) and the particles average diameter, respectively (Mohamed et al., 2021; Singh et al., 2019).

2.4. Photocatalytic performance of quantum dots oxide samples

The first method used to evaluate the photocatalytic activity performance of the ZQs prepared samples is the photodegradation process of the Indigo Carmine dye as a selective industrial textile dye. 0.5 g/L of the prepared ZQs samples were dispersed in 100 ml of Indigo Carmine dye solution (5×10–5 M) at pH = 6.6 during the experimental procedures (Wahba et al., 2020). The dye solution was stirred in the dark-room for 15 min in the presence of the prepared samples to detected the adsorption–desorption equilibrium. A photoreactor used in the photodegradation process has a xenon arc lamp as a light source (from the Engineering Firm, Egypt). Also, a water-cooling cycle system is used in the reactor to remove the lamp temperature effect. The Xenon lamp has suitable power strength for this proposal which is 100 W/Cm^2 and its wavelength limits between 100 and 1100 nm. The photodegradation test was investigated under the Xenon light bulb as a light source which the ZQ's particles are extracted in the final step of photodegradation after the illumination process, centrifuged for a further 15 min at 8000 rpm.

Total organic carbon (TOC) of the investigated dye and factory effluents samples after the photodegradation processes is measured by the TOC analyzer (Model TOC-VCPH from Shimadzu Firm) to determine the maximum photodegradation percentage for each sample.

Also, the fluorescence rate of 7-Hydroxychromen-2-one (coumarin) photooxidation is the second way of estimating the photocatalytic performance of the ZQs prepared samples. The experiment starts with the preparation of both coumarin solution (0.146 g/L), referred to as (solution A), and the catalysts prepared solution (ZQs) (0.5 g/L), referred to as (solution B). Then mixed solution B which is dissolved in solution A and vigorously stirred at the UV source. Fluorescence spectrum emissions have been measured over a specific period after revealed the light at solution excitation (λ_{ex} = 332 nm). The results indicate that under these parameters, coumarin is not active.

Finally, the solar photocatalytic process for dyes with a high environmental hazard is considered an interesting application to evaluate the photocatalytic activity performance of the ZQs prepared samples. The procedure was carried out at pH 7 (neutral medium) under sunlight as the third approach for photocatalytic activity efficiency for samples prepared by ZQs.

During this analysis, the sunlight doze has 2.9 mW/Cm^2 and 1091 mW/Cm^2 of UV radiation and visible light, respectively. Also, the mineralization efficiency determined by using of COD 'C-99′ model - HANNA Company and as the following formula

$$\text{Efficiencyofmineralization} = \frac{\text{CODo} - \text{CODt}}{\text{CODo}} \times 100 \quad (2)$$

where COD_0 and COD_t are the chemical oxygen demand at zero and time t, respectively.

3. Results and discussion

3.1. XRPD-Characterization

Analysis of X-ray powder diffraction (XRPD) is a distinguishable way to evaluate the crystalline phases and structure of ZQs prepared samples. The resulting evidence gives direct proof of the single wurtzite crystal phase structure of the prepared ZQS compared to the crystallographic data for index card No. 36–1451 in the JCPDS-ICDD. With the two theta values of 31.67, 34.4, 36.2, 47.58, 56.47, 62.61, and 67.92^0, the major characteristic XRPD peaks of the ZQs prepared samples observed to belong to the following planes of (100), (002), (101), (102), (110), (103) and (112), respectively (Fig. 1 (a)).

The lack of any additional diffraction peaks in the pattern indicated the superior purity of the samples. The prepared quantum dot samples are similar depending on the relative refinement technique and have the same packing structure as represented in Fig. 1 (b). The Debye-Scherer equation was applied with the following formula to calculate the crystallite size (D) of the prepared ZQs (Mohamed et al., 2020).

$$D = 0.89\lambda/\beta\cos\theta \quad (3)$$

Where the symbols λ, β and θ represent the wavelength radiation of the X-ray radiation, the full width at the half-peak maximum (FWHM), and the maximum peak position of the diffraction angle, respectively, the Scherrer constant is 0.9 (Fan et al., 2013; Mohamed et al., 2020; Yang et al., 2016). The calculated results obtained indicate a decrease in the mean crystallite size value for the first ZQ1 sample (4.4 nm) compared to the second ZQ2 sample (5.3 nm) shown in Fig. 1 (c), which has XRPD demonstrator parameters for the ZQ1 and ZQ2.

3.2. TEM

High-resolution transmission electron microscopy was a potent and effective way to investigate surface morphology and the particle size of ZQ2 prepared samples. The superfine nanoparticles, extreme crystallinity composition, and ellipsoidal elongated shape are in Fig. 2. This observation forms one of the most outstanding surface qualities for the prepared samples.

The observed average particle size is 4.4 nm and 5.3 nm for the samples ZQ1 and ZQ2, respectively, was determined by using the Debye-Scherer equation. These results indicate

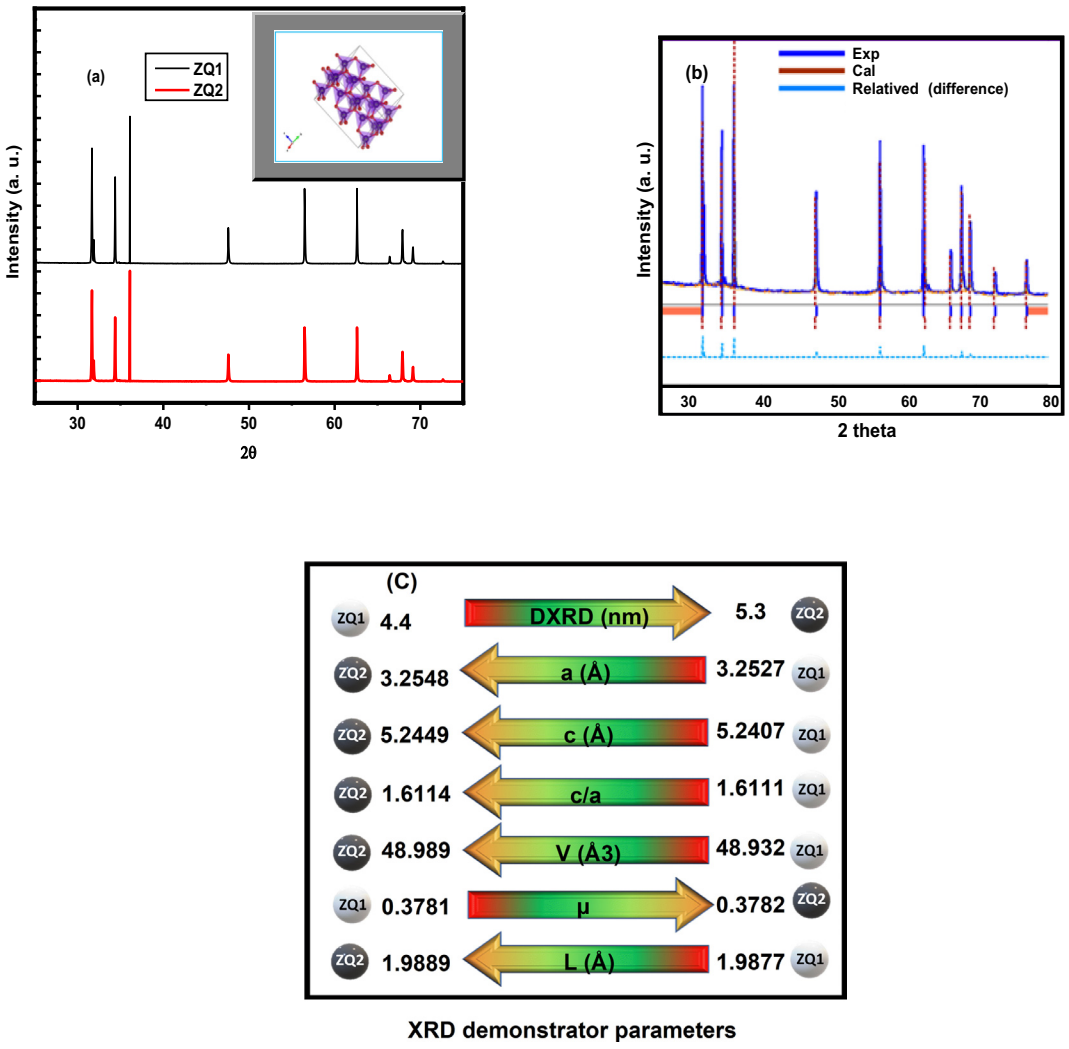

Fig. 1 XRPD (a), relative refinements (b) and XRPD demonstrator parameters (c) for ZQs prepared samples.

increases in the hydroxyl volume during the preparation process, leading to increases in particle size of the prepared samples.

The approximate crystallite size values calculated by HRTEM images give significantly higher values by 10% from the actual size than that measured by XRPD, it may be due to the limited agglomeration found for the prepared quantum dot samples as a result of aging the samples until they measured.

3.3. Bandgap energies

Using Ultraviolet–visible absorption spectroscopy of the optical properties of the prepared catalysts was carried out. The absorption spectra of the prepared ZQ2 sample are greater than those of the ZQ1, as seen in Fig. 2, which shows the significant impact of the additional hydroxide concentrations in the prepared samples. One of the interesting features derived from the optical analysis is the determination of energy bandgap values due to its significant effect on the photocatalytic behavior of ZQs samples.

Tauc's gap equation was employed to measure the optical bandgap energies by any of the following formulas:

$$\alpha = \beta/h\upsilon\left(h\upsilon - E_g\right)^n \text{or} (\alpha h\upsilon)^{1/n} = \beta\left(h\upsilon - E_g\right) \tag{4}$$

$$\text{Whichcanbeexpressedas} (\alpha h\upsilon)^2 = A\left(h\upsilon - E_g\right) \tag{5}$$

where E_g, A, n, hυ, β and α is optical bandgap energy, constant, power factor of the transition mode, photon energy, band tailing parameter constant and the absorption coefficient, respectively.

The measuring process of the second relationship generates a clear line in a lower region of the curve when photon energy (hυ) plotted against $(\alpha h\upsilon)^2$, where the bandgap (E_g) values obtained by crossing the extrapolation of the corresponding straight line with the axis of hυ. ZQs samples prepared in Fig. 3, 3.53 eV, and 3.50 eV were showed for ZQ1 and ZQ2 samples, respectively. By comparison to (3.37 eV) for the bulk ZnO. These results appear when a distinctive quantum effect (quantum confinement effect) and the change in the blue area of the absorption band are detected.

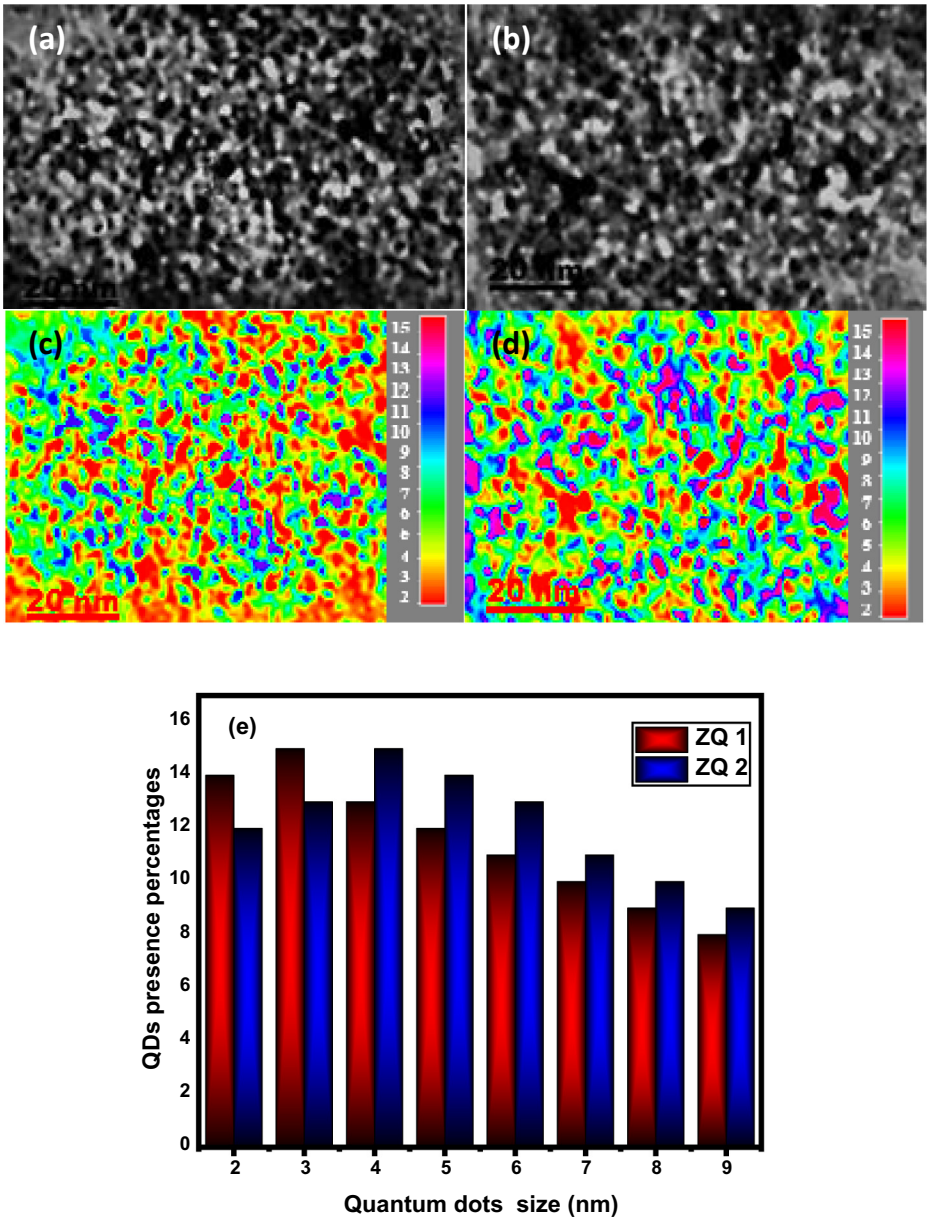

Fig. 2 TEM image of ZQs prepared samples (a and b) along with their particle size distribution map (c and d) and QDs presence percentages (e).

From absorption spectra, as shown in Fig. 3 (b), A small blue shift from 370 to 374 nm observed indicate increases in frequency within decreasing in wavelength, the observed tunning due to decreases ZQs particle size. On the other side, from the emission spectra (Fig. 3 (c)), a distinguishable blue shift was observed nearly about 11 nm from 550 to 561 nm, which is excitation wavelength decreased from 374 to 370 nm as shown in Fig. 3 (b). This observation is expected as the same blue shift observed in the absorption spectra due to the decrease in the ZQs size from ZQ2 (5.3 nm) to ZQ1(4.4 nm). Triggering as an additional factor of ZQs surface-functionalized may be led to a decrease and/or increase of the defects of the ZQs surface (van Dijken et al., 2000). A broad emission band occurred by a defined type of electronic relaxation observed when trapping inside the surface $O2^{-}$/O^{-} states occurred by the photo-generated holes. Trapped holes formed during tunneling processes and subsequent recombination with the oxygen vacancies can return to the bulk phase or larger ZQs size (from ZQ1 to ZQ2). This observation led to the emission effect is more intense for the smaller ZQs size (ZQ1) according to the observed recombination in the visible range (Ambade et al., 2014; van Dijken et al., 2000).

Also, UV–vis diffuse reflectance spectra presented in (Fig. 3 (d)) suggest very low reflection rate in the visible region; thus, verifying the amount of light absorption by ZQ1 is higher as compared to ZQ2. This observation due to the photocatalytic activity of ZQ1 is higher than ZQ2 because of ZQ1 is the smaller in size and larger in surface area than ZQ2.

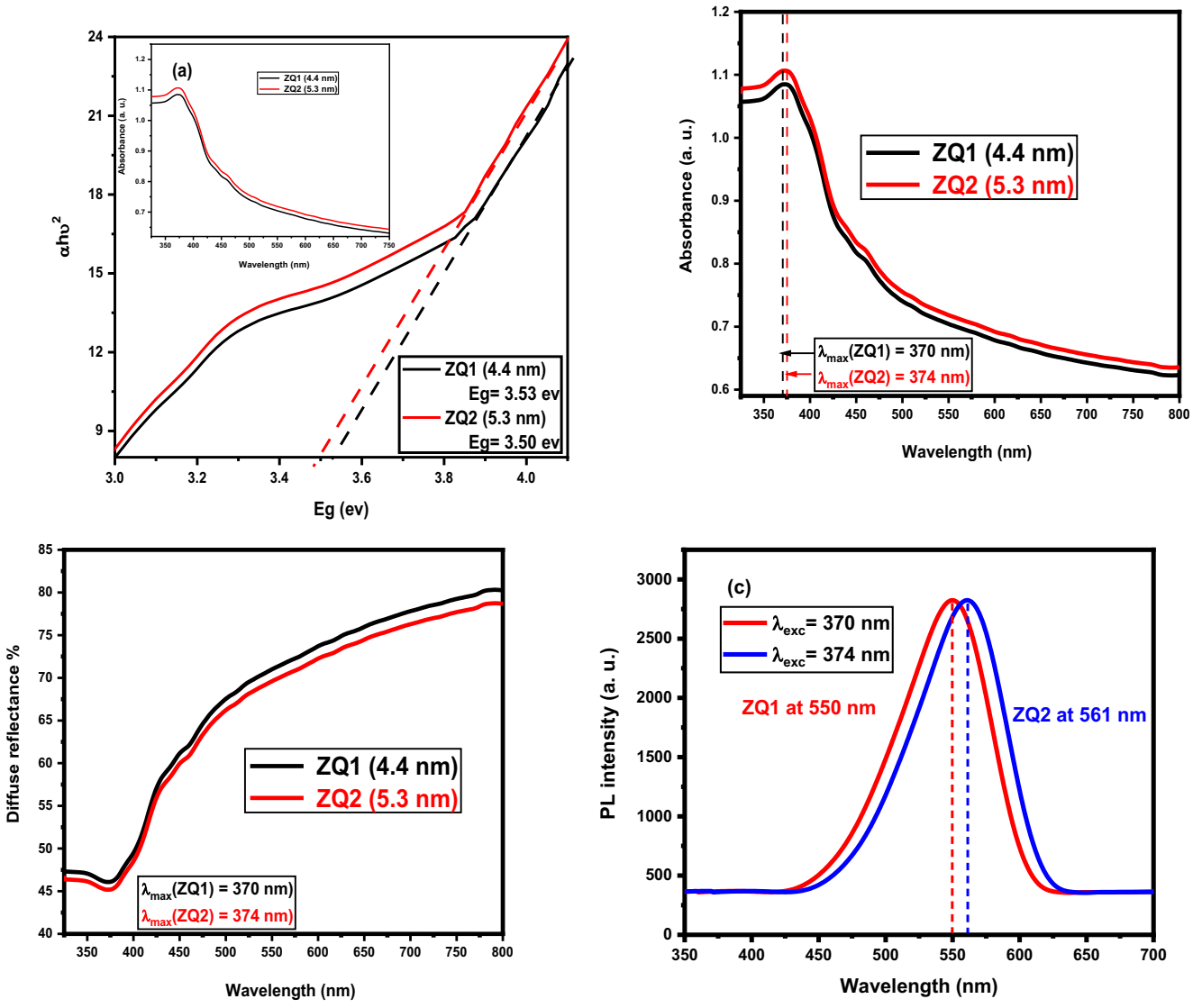

Fig. 3 Band gap energies (a), absorption spectra (b), emission spectra (c) and UV-DRS spectra (d) of ZQs samples.

3.4. Surface area (BET)

Large surface areas observed are considered one of the most distinctive surface characteristics due to identify the efficiency and performance of photocatalysts prepared for various applications. The BET theory is an outstanding instrument to measure the surface (S) of ZQs prepared samples. For the ZQ 1 and ZQ 2 tests, the approximate surface area values are 233.25 and 197.81 m^2/g. The relation between BET, E_g, and quantum particle size values seen for each of the ZQ samples (Fig. 4). These results demonstrate that the reduction in the optical bandgap and the particle size led to increasing the surface area affected by hydroxyl ion lack.

3.5. Photocatalytic activity of ZQs

The photocatalytic assessment of ZQs prepared samples using three applications of manufacturing, economic and environmental significance.

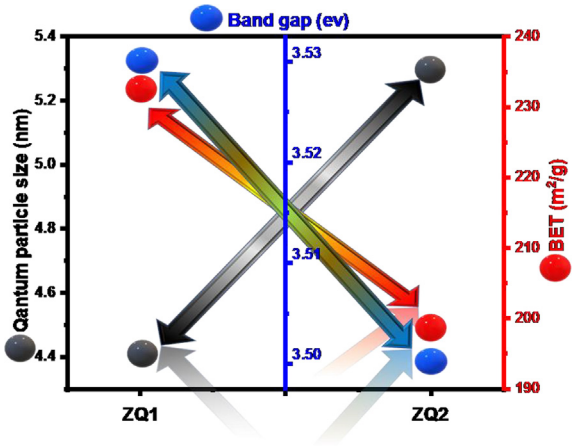

Fig. 4 Correlation between quantum particle size, E_g and BET of ZQs samples.

Indigo Carmine (IC) is one of the commercially organic dyes consumed in the food and garment industry in Egypt. The safe handling is an important environmental issue to assess the catalytic efficiency of ZQs prepared samples via the IC dye photodegradation process, multiple experiments, and relationships are determined.

The first evaluation way is the changes in the absorbance spectra of the dye within the different degradation periods under xenon lamp irradiation as a light source, as seen in Fig. 5, demonstrating the linear relationships between ln (C_o/C_t) with irradiation time for the photodegradation process. Also, the photodegradation process reaction rate constant (K_{app}) was determined using formulas (6).

Both ZQ1 and ZQ2 have equal overall photodegradation percentages of 99.93 and 99.91, respectively. But ZQ1 has a higher photodegradation rate than ZQ2, 17.18 × 10^{-3}, and 15.25 × 10^{-3}, respectively. It refers to the improvement of the photodegradation rates accompanied by decreases in the photodegradation times and quantum particle size seen in Fig. 5. Concurrently, the results demonstrate that the excellent photodecontamination rate is directly proportional to the minimum time needed for photodegradation, active surface area, and energy gap. Also, the photodecontamination rate is inversely proportional to the average size of the ZQs particles (Fig. 6).

The starting point of the suggested mechanism for the IC dye photodegradation process in presence of the prepared samples is in the valence band (VB) region, where the electrons are transferred to the conduction band (CB) region when the catalyst exposure to the light source. This process will result in the relocation of the electron to the upper level of exciting negative electrons (e^-), while at the lower level a positive hole (h^+) formed at the previous level. So, the reactive species formed due to superoxide and hydroxyl radicals created by the reaction of e- and h + with the oxygen (O2) and water (H2O) molecules, respectively. By targeting the subsequent active components of the target IC dye molecule, the degradation mechanism completed and the full photodegradation mechanism is published in our previous work (Mohamed et al., 2020; Ambade et al., 2014; Foo et al., 2014; Hirai et al., 2005; Wahba et al., 2020).

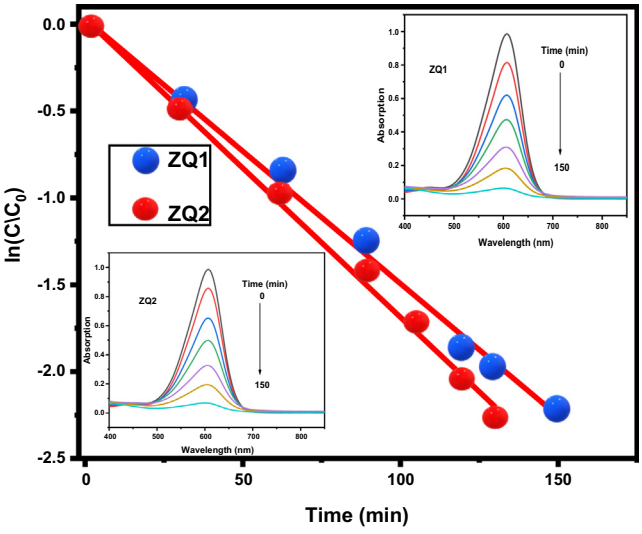

Fig. 5 Kinetics photodegradation rate plot of Indigo Carmine dye in presence of ZQs.

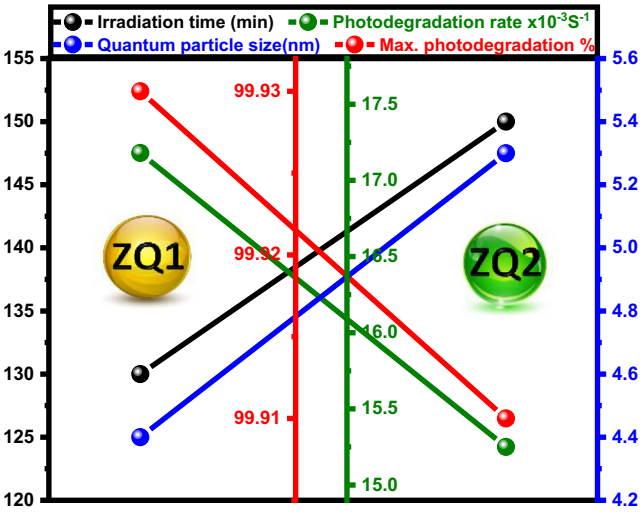

Fig. 6 Correlation between irradiation times, max. photodegradation percentages, Photodegradation rates and quantum particle size of ZQs prepared samples.

Under the previous condition, ZQs prepared samples are revealed to a substantial improvement for the photodegradation process by shortening the recombination step time required led to increases in the photodegradation rate of the investigated dye. TOC analysis determines the highest percentage of organic carbon disappearance (dissociation) during the photodegradation processes seen in Fig. 7.

A phenolic organic compound belonging to the Coumarin family is 7-Hydroxychromen-2-one, which has numerous biological applications such as anti-microbial, anti-oxidant, and anti-carcinogenic cells. The photo-oxidation process of Coumarin (7-hydroxychromen-2-one) is the second way of testing the photocatalytic behavior of ZQs by the fluorescent probe instrument. Fig. 8 shows the effect of the photocatalysts on the coumarin emission spectra and fluorescence rate constant (K_f) under illumination with UV light for one hour. A pseudo-zero-order reaction followed because the photo-oxidation rate improved in the first sample than the second sample as in the IC dye photodegradation process and the values listed in Table 1.

Coumarin dye oxidation boosted in the presence of the ZQ1 (4.4 nm) sample, which is the smallest particle size prepared sample. ZQ1 has a high energy bandgap (3.53 eV), the area of the surface (233.25 m^2/g), the rate of fluorescence (51.46 × 10^{-3}), apparent OH radical formation rate (35.91 × 10^{-3}), and have a greater e-/h + pair separation efficiency than that of ZQ2 (5.3 nm) sample. All above results have a distinguishable performance compared to literature and our previous work (Mohamed et al., 2021; Chen et al., 2019; Mohamed et al., 2020;).

3.6. Solar photocatalytic process for hazardous factory effluents

Industrial waste and especially wastewater contain many organic dyes, which are known for their high degradation resistance. They are a source of many environmental and

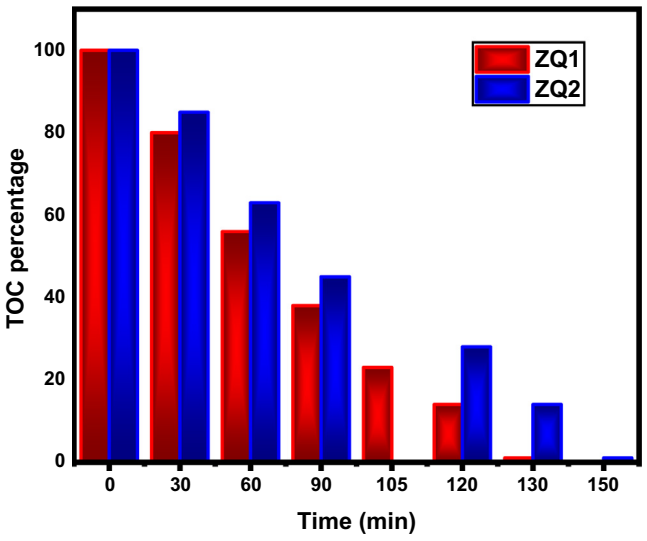

Fig. 7 TOC analysis for photodegradation process of Indigo Carmine in presence of ZQs.

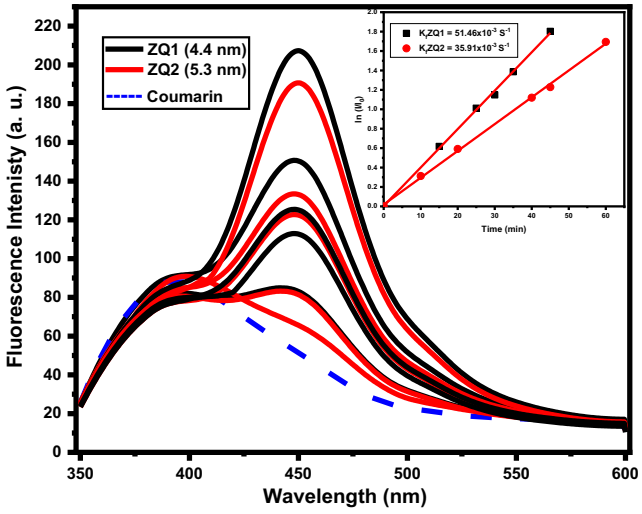

Fig. 8 Emission spectra of coumarin in presence of different ZQs samples.

health issues under normal conditions. Organic effects on waste are measured using an accurate study of the need for chemical oxygen to detect the amount of oxygen needed to turn organic waste into environmentally safe end products (CO_2 and H_2O). Organic waste is measured by chemical oxygen demand (COD).

The particle size was the main factor effect in COD values for the wastewater sample estimated during the wastewater treatment process (Fig. 9). The reported results aligned to the safe limits of the environmental law of Egypt (COD $<$1000 ppm) (2009).

January-February an experimental investigation period with one of the largest Egyptian Spinning & Weaving companies that showed high COD values ranging between 4215 and 6138 (ppm) shown in Table 2.

It can clarify from the results obtained that the spectrum of COD values for 16 COD investigated samples for hazardous factory effluents as industrial wastewater samples allowed a cap for the use of ZQ1 (4.4 nm) as a photocatalyst except for NO. 13 and NO. 4, 11, and 13 for ZQ2 (5.3). But there are seven samples in the risky limit range (901 to 978) for ZQ2 and only two samples for ZQ1. From the above findings, better results were obtained for the smallest particle size ZQ1 than ZQ2, which leads to an improvement in industrial wastewater mineralization. (photodegradation) over an assess-

Table 1 Photodegradation rates (K_{app}) and Fluorescence rate (K_f) constants for ZQs prepared samples.

	(ZQ1 = 4.4 nm)	(ZQ2 = 5.3 nm)
K_{app}	17.18×10^{-3}	15.25×10^{-3}
K_f	51.46×10^{-3}	$(35.91x\ 10^{-3}$

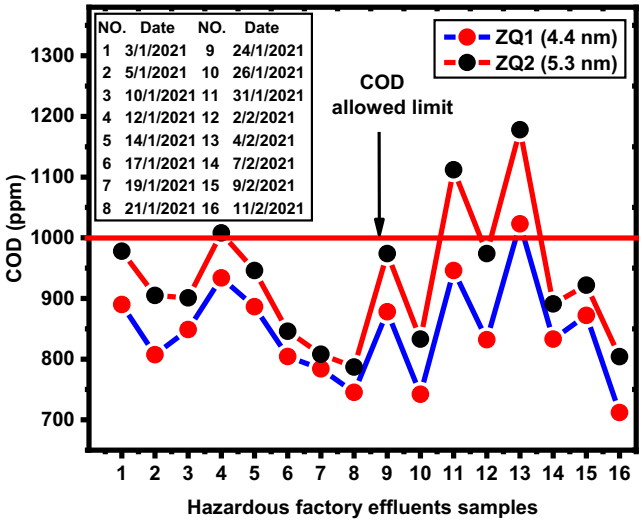

Fig. 9 COD evaluation for industrial wastewater in presence of ZQs prepared samples.

Table 2 COD values for solar photocatalytic process of industrial wastewater samples in 2021 in presence of ZQs prepared samples.

No. of recycling process		1	2	3	4	5	6	7	8	9	10	11	12	13	14	15	16
Samples Date		3 Jan.	6 Jan.	10 Jan.	12 Jan.	14 Jan.	17 Jan.	19 Jan.	21 Jan.	24 Jan.	26 Jan.	31 Jan.	2 Feb.	4 Feb.	7 Feb.	9 Feb.	11 Feb.
Actually COD		5320	4822	5078	5588	5310	4804	4700	4450	5238	4442	5636	4982	6138	4990	5242	4215
COD Value (ppm)	ZQ1	890	807	848	933	886	804	784	745	878	742	942	832	1023	833	872	712
	ZQ2	978	905	901	1008	946	846	808	787	974	833	1112	974	1178	891	922	804

Color key		Upper limit		Risky limit		Allowed limit

ment period owing to an increase in photo-oxidation processes with a decrease in quantum particle size. From the above results, there are 13 samples from 16 investigated factory effluents samples subject to the allowed COD limit (less than 899 ppm) for ZQ1 but only six samples in case of ZQ2 in the allowed COD limit.

The future work plan is to use various forms of ZnO depending on their particle sizes as quantum dots or nanoparticles to be economical. Prospective future research would also provide a local economic strategy for ZQ preparation since there are more exciting uses for ZQs as sophisticated new optics and solar cell applications.

3.7. Recycling of ZQs during industrial wastewater treatment of factory effluents

The recycling method is one of the more effective studies in the economic and environmental sector for preserving and repeatedly using prepared catalysts for two photocatalytic activity evaluation processes for both Indigo Carmine and industrial wastewater of factory effluents.

Indigo Carmine destruction occurred was replicated ten times using a variety of (ZQs) prepared samples with a concentration (0.5 g/l). The photodegradation rates were decreased by 36.5 % from (17.18×10^{-3} to 10.92×10^{-3}) and 38.5 % from (15.25×10^{-3} to 9.41×10^{-3}) in the presence of ZQ1 and ZQ2 samples, respectively (Fig. 10 (a and b). The correlation curve between repetitions using the number of various prepared ZQ samples and the photodegradation rates of Indigo Carmine dye shown in (Fig. 10 (c)). Also, nanofiltration membranes used to avoid any weight loss, so the repetition (recycling) reached to 10 times with high photocatalytic efficiency for the photocatalysts prepared. The regular accumulation of catalysts is the explanation key for the depression rate, which eventually results in the reduction of photocatalytic activity that can be seen in the ZQ2 than ZQ1 sample, indicating the impact of the particle size on the effectiveness of the prepared materials.

The recycling process for the solar photocatalytic process of industrial wastewater samples depended on using ZQs as a photocatalyst. Also, the recycling process efficiency has been investigated by determining COD values at ten replicate times for industrial wastewater recycling in the Egyptian Spinning and Weaving Company as shown in Table 3 and 10 (d).

Aggregation of the prepared ZQs samples during the recycling process led to decreased recycling activity because increasing its particle size due to decreases in its active surface area. These findings were observed because ZQ samples prepared behaved like a very interesting active photocatalyst.

4. Conclusion

Evaluation of the photocatalytic efficiency of ZQs samples prepared by easily modified precipitation method determined for the Indigo Carmine dye (as organic hazardous materials), and 16 factory effluents investigated samples (as industrial wastewater samples). All results refer to ZQ1 as a very active photocatalyst during the photodegradation process and solar photocatalytic process, which verified by the recycling process (repeat for ten times) of the use of ZQ1 and ZQ2. During all various photocatalytic reactions, the ZQ1 has superior efficiency and higher photodegradation rate for Indigo Carmine dye and factory effluents samples than the ZQ2 due to the distinctive photophysical features of ZQ1 which has the smallest quantum particle size (4.4 nm) than the ZQ2 size (5.3 nm). Also, the reduction in the optical bandgap and the particle size led to increasing the surface area affected by hydroxyl ion lack which due to improvement the photodegradation rates done by ZQ1 than ZQ2 during all photodegradation processes by xenon reactor and solar photocatalytic process.

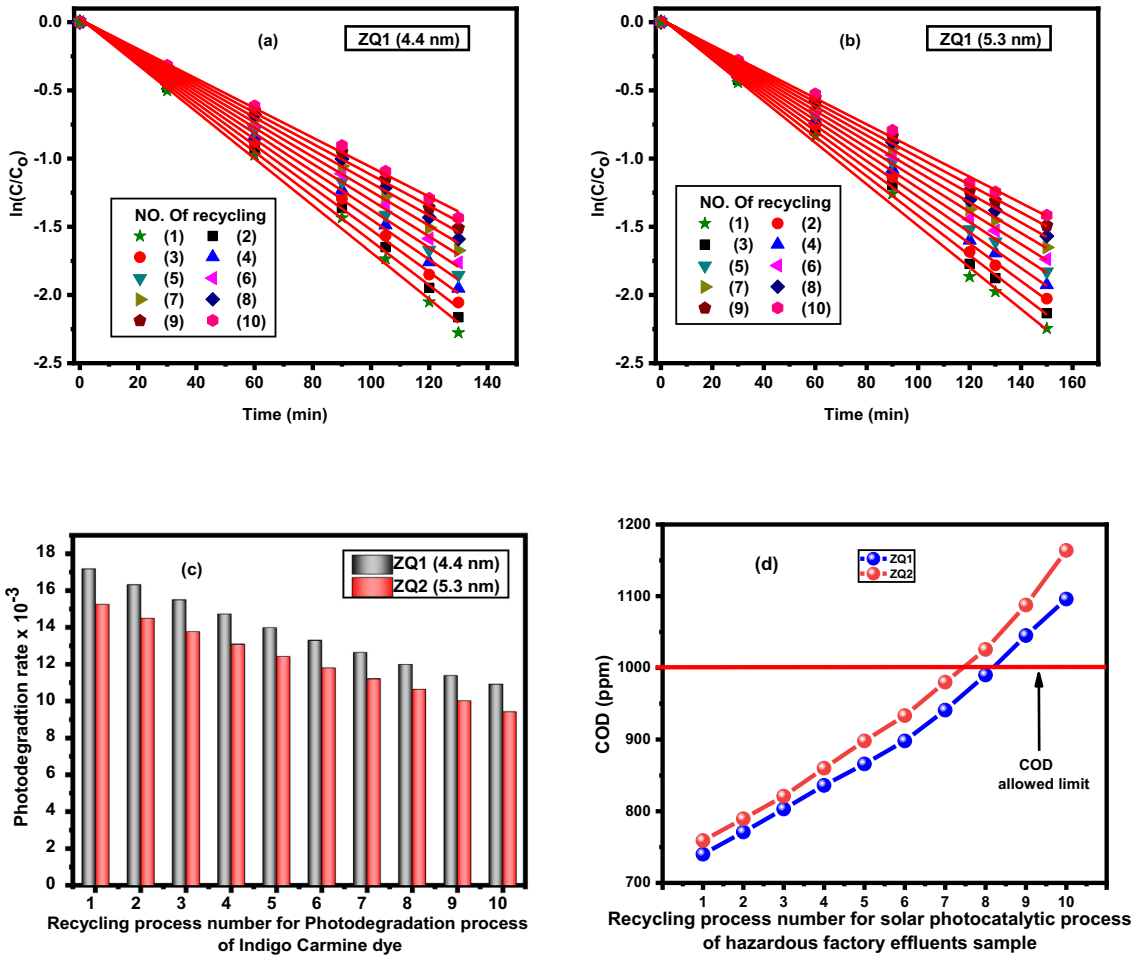

Fig. 10 (a and b) photodegradation rates, (c) Correlation between recycling process number and photodegradation rate of Indigo Carmine dye and (d) COD limits for recycling process.

Table 3 COD values for recycling process of industrial wastewater in presence of ZQs samples.

No. of recycling process		1	2	3	4	5	6	7	8	9	10
COD Value (ppm)	ZQ1	740	771	803	836	866	898	941	990	1045	1096
	ZQ2	762	794	827	868	908	945	994	1042	1107	1187

Color key		Upper limit		Risky limit		Allowed limit

Declaration of Competing Interest

The authors declare that they have no known competing financial interests or personal relationships that could have appeared to influence the work reported in this paper.

Acknowledgements

"The authors extend their appreciation to the Deanship of Scientific Research at King Khalid University for funding this work through General Research Project under grant number (RGP. 1/287/42)."

References

9. ENVIRONMENTAL CHANGE. The Egyptian Journal of Environmental Change 1, 1-2.https://doi.org/10.21608/ejec.9.96541

Abo Zeid, E.F., Ibrahem, I.A., Mohamed, W.A.A., Ali, A.M., 2020. Study the influence of silver and cobalt on the photocatalytic activity of copper oxide nanoparticles for the degradation of methyl orange and real wastewater dyes. Materials Research Express 7, 026201.https://doi.org/10.1088/2053-1591/ab7400

Alexandrov, A., Zvaigzne, M., Lypenko, D., Nabiev, I., Samokhvalov, P., 2020. Al-, Ga-, Mg-, or Li-doped zinc oxide nanoparticles as electron transport layers for quantum dot light-emitting diodes. Sci. Rep. 10, 7496. https://doi.org/10.1038/s41598-020-64263-2.

Ambade, S.B., Ambade, R.B., Kim, S., Park, H., Yoo, D.J., Lee, S.-H., 2014. Performance Enhancement in Inverted Solar Cells by Interfacial Modification of ZnO Nanoparticle Buffer Layer. J. Nanosci. Nanotechnol. 14, 8561–8566. https://doi.org/10.1166/jnn.2014.9996.

Banerjee, S., Pillai, S.C., Falaras, P., O'Shea, K.E., Byrne, J.A., Dionysiou, D.D., 2014. New Insights into the Mechanism of Visible Light Photocatalysis. J. Phys. Chem. Lett. 5, 2543–2554. https://doi.org/10.1021/jz501030x.

Busseron, E., Ruff, Y., Moulin, E., Giuseppone, N., 2013. Supramolecular self-assemblies as functional nanomaterials. Nanoscale 5, 7098. https://doi.org/10.1039/c3nr02176a.

Chen, C., Liu, X., Long, H., Ding, F., Liu, Q., Chen, X.a., 2019. Preparation and photocatalytic performance of graphene Oxide/WO3 quantum Dots/TiO2@SiO2 microspheres. Vacuum 164, 66–71. https://doi.org/10.1016/j.vacuum.2019.03.002.

El-Sayed, B.A., Mohamed, W.A.A., Galal, H.R., Abd El-Bary, H.M., Ahmed, M.A.M., 2019. Photocatalytic study of some synthesized MWCNTs/TiO_2 nanocomposites used in the treatment of industrial hazard materials. Egypt. J. Pet. 28, 247–252. https://doi.org/10.1016/j.ejpe.2019.05.002.

Fan, F., Feng, Y., Bai, S., Feng, J., Chen, A., Li, D., 2013. Synthesis and gas sensing properties to NO2 of ZnO nanoparticles. Sens. Actuators, B 185, 377–382. https://doi.org/10.1016/j.snb.2013.05.020.

Felbier, P., Yang, J., Theis, J., Liptak, R.W., Wagner, A., Lorke, A., Bacher, G., Kortshagen, U., 2014. Highly Luminescent ZnO Quantum Dots Made in a Nonthermal Plasma. Adv. Funct. Mater. 24, 1988–1993. https://doi.org/10.1002/adfm.201303449.

Foo, K.L., Kashif, M., Hashim, U., Liu, W.-W., 2014. Effect of different solvents on the structural and optical properties of zinc oxide thin films for optoelectronic applications. Ceram. Int. 40, 753–761. https://doi.org/10.1016/j.ceramint.2013.06.065.

Hanna, A.A., Mohamed, W.A.A., Ibrahim, I.A., 2014. Studies on Photodegradation of Methylene Blue (MB) by Nano-sized Titanium Oxide. Egypt. J. Chem. 57, 315–325. https://doi.org/10.21608/ejchem.2014.1055.

Hirai, T., Harada, Y., Hashimoto, S., Itoh, T., Ohno, N., 2005. Luminescence of excitons in mesoscopic ZnO particles. J. Lumin. 112, 196–199. https://doi.org/10.1016/j.jlumin.2004.09.055.

Jain, A., Panwar, S., Kang, T.W., Jeon, H.C., Kumar, S., Choubey, R. K., 2014. Effect of zinc oxide concentration in fluorescent ZnS:Mn/ZnO core–shell nanostructures. J. Mater. Sci.: Mater. Electron. 25, 1716–1723. https://doi.org/10.1007/s10854-014-1788-3.

Khan, R., Hassan, M.S., Jang, L.-W., Hyeon Yun, J., Ahn, H.-K., Khil, M.-S., Lee, I.-H., 2014. Low-temperature synthesis of ZnO quantum dots for photocatalytic degradation of methyl orange dye under UV irradiation. Ceram. Int. 40, 14827–14831. https://doi.org/10.1016/j.ceramint.2014.06.076.

Kharkwal, A., Purohit, G., Rahul, Rawat, D.S., 2020. Zinc Oxide Sensitized Graphene Quantum Dots "ZnO-GQDs": A Hybrid Concept to Study Charge Transfer and its Catalytic Applicability to Synthesize Tetrasubstituted Propargylamines. Asian Journal of Organic Chemistry 9, 2162-2169.https://doi.org/https://doi.org/10.1002/ajoc.202000460

Kitture, R., Pawar, D., Rao, C.N., Choubey, R.K., Kale, S.N., 2017. Nanocomposite modified optical fiber: A room temperature, selective H2S gas sensor: Studies using ZnO-PMMA. J. Alloy. Compd. 695, 2091–2096. https://doi.org/10.1016/j.jallcom.2016.11.048.

Kumar, A., Kumar, M., Bhatt, V., Kim, D., Mukherjee, S., Yun, J.-H., Choubey, R.K., 2021a. ZnS microspheres-based photoconductor for UV light-sensing applications. Chem. Phys. Lett. 763, 138162. https://doi.org/10.1016/j.cplett.2020.138162.

Kumar, S., Jeon, H.C., Kang, T.W., Seth, R., Panwar, S., Shinde, S. K., Waghmode, D.P., Saratale, R.G., Choubey, R.K., 2019. Variation in chemical bath pH and the corresponding precursor concentration for optimizing the optical, structural and morphological properties of ZnO thin films. J. Mater. Sci.: Mater. Electron. 30, 17747–17758. https://doi.org/10.1007/s10854-019-02125-y.

Kumar, S., Kavita, Bhatti, H.S., Singh, K., Gupta, S., Sharma, S., Kumar, V., Choubey, R.K., 2021b. Effect of glutathione capping on the antibacterial activity of tin doped ZnO nanoparticles. Physica Scripta 96, 125807.https://doi.org/10.1088/1402-4896/ac1eb3

Lee, D., Wolska-Pietkiewicz, M., Badoni, S., Grala, A., Lewiński, J., De Paëpe, G., 2019. Disclosing Interfaces of ZnO Nanocrystals Using Dynamic Nuclear Polarization: Sol-Gel versus Organometallic Approach. Angew. Chem. 131, 17323–17328. https://doi.org/10.1002/ange.201906726.

Liang, H., Tai, X., Du, Z., Yin, Y., 2020. Enhanced photocatalytic activity of ZnO sensitized by carbon quantum dots and application in phenol wastewater. Opt. Mater. 100, 109674. https://doi.org/10.1016/j.optmat.2020.109674.

Lin, Y., Hong, R., Chen, H., Zhang, D., Xu, J., 2020. Green Synthesis of ZnO-GO Composites for the Photocatalytic Degradation of Methylene Blue. Journal of Nanomaterials 2020, 1-11.https://doi.org/10.1155/2020/4147357

Mohamed, W.A.A., Handal, H.T., Ibrahem, I.A., Galal, H.R., Mousa, H.A., Labib, A.A., 2021. Recycling for solar photocatalytic activity of Dianix blue dye and real industrial wastewater treatment process by zinc oxide quantum dots synthesized by solvothermal method. J. Hazard. Mater. 404, 123962. https://doi.org/10.1016/j.jhazmat.2020.123962.

Mohamed, W.A.A., Ibrahem, I.A., El-Sayed, A.M., Galal, H.R., Handal, H., Mousa, H.A., Labib, A.A., 2020. Zinc oxide quantum dots for textile dyes and real industrial wastewater treatment: Solar photocatalytic activity, photoluminescence properties and recycling process. Adv. Powder Technol. 31, 2555–2565. https://doi.org/10.1016/j.apt.2020.04.017.

Mohammed Ali, M.J., Chauveau, J.M., Bretagnon, T., 2018. Evidence of exciton complexes in non polar ZnO/(Zn, Mg)O A-plane quantum well. Superlattices Microstruct. 120, 410–418. https://doi.org/10.1016/j.spmi.2018.05.067.

Muşat, V., Tăbăcaru, A., Vasile, B.Ş., Surdu, V.-A., 2014. Size-dependent photoluminescence of zinc oxide quantum dots through organosilane functionalization. RSC Adv. 4, 63128–63136. https://doi.org/10.1039/c4ra10851e.

Nandi, P., Das, D., 2019. Photocatalytic degradation of Rhodamine-B dye by stable ZnO nanostructures with different calcination temperature induced defects. Appl. Surf. Sci. 465, 546–556. https://doi.org/10.1016/j.apsusc.2018.09.193.

Rani, G., Sahare, P.D., 2013. Structural and Spectroscopic Characterizations of ZnO Quantum Dots Annealed at Different Temperatures. J. Mater. Sci. Technol. 29, 1035–1039. https://doi.org/10.1016/j.jmst.2013.08.015.

Repp, S., Erdem, E., 2016. Controlling the exciton energy of zinc oxide (ZnO) quantum dots by changing the confinement conditions. Spectrochim Acta A Mol Biomol Spectrosc 152, 637–644. https://doi.org/10.1016/j.saa.2015.01.110.

Senger, R.T., Bajaj, K.K., 2003. Binding energies of excitons in polar quantum well heterostructures. Phys. Rev. B, 68. https://doi.org/10.1103/PhysRevB.68.205314.

Singh, S., Kumar, V., Romero, R., Sharma, K., Singh, J., 2019. Applications of Nanoparticles in Wastewater Treatment. Nanobiotechnol. Bioformulations Springer International Publishing, 395–418.

Tanji, K., Navio, J.A., Chaqroune, A., Naja, J., Puga, F., Hidalgo, M. C., Kherbeche, A., 2020. Fast photodegradation of rhodamine B and caffeine using ZnO-hydroxyapatite composites under UV-light illumination. Catalysis. https://doi.org/10.1016/j.cattod.2020.07.044.

Vaez, Z., Javanbakht, V., 2020. Synthesis, characterization and photocatalytic activity of ZSM-5/ZnO nanocomposite modified by Ag nanoparticles for methyl orange degradation. J. Photochem. Photobiol., A 388, 112064. https://doi.org/10.1016/j.jphotochem.2019.112064.

van Dijken, A., Meulenkamp, E.A., Vanmaekelbergh, D., Meijerink, A., 2000. The luminescence of nanocrystalline ZnO particles: the mechanism of the ultraviolet and visible emission. J. Lumin. 87–89, 454–456. https://doi.org/10.1016/s0022-2313(99)00482-2.

Wahba, M.A., Yakout, S.M., Mohamed, W.A.A., Galal, H.R., 2020. Remarkable photocatalytic activity of Zr doped ZnO and ZrO2/ZnO nanocomposites: Structural, morphological and photoluminescence properties. Mater. Chem. Phys. 256, 123754. https://doi.org/10.1016/j.matchemphys.2020.123754.

Wang, S., Lin, S., Zhang, D., Li, G., Leung, M.K.H., 2017. Controlling charge transfer in quantum-size titania for photocatalytic applications. Appl. Catal. B 215, 85–92. https://doi.org/10.1016/j.apcatb.2017.05.043.

Yang, W., Zhang, B., Ding, N., Ding, W., Wang, L., Yu, M., Zhang, Q., 2016. Fast synthesize ZnO quantum dots via ultrasonic method. Ultrason. Sonochem. 30, 103–112. https://doi.org/10.1016/j.ultsonch.2015.11.015.

Zhu, C., Yang, Y.-Y., Zhao, Z.-G., 2018. Surface voltammetric dealloying investigation on PdCu/C electrocatalysts toward ethanol oxidation in alkaline media. J. Nanopart. Res. 20, 314. https://doi.org/10.1007/s11051-018-4423-z.